Light particle-evaporation residue coincidences for the ^{79}Br+^{27}Al system at 11.8 MeV/nucleon

J. Gomez del Campo, D. Shapira, M. Korolija, H. J. Kim, K. Teh,* and J. Shea†
Oak Ridge National Laboratory, Oak Ridge, Tennessee 37831

J. P. Wieleczko
Grand Accelerateur National d'Ions Lourds, Boîte Postale 5133, 14040 Caen CEDEX, France

E. Chávez, M. E. Ortiz, and A. Dacal
Instituto de Física Universidad Nacional Autónoma de México, Mexico 01000 D.F., Mexico

C. Volant
DAPNIA/SPhN CEN-Saclay, 91191 Gif-sur-Yvette, Cedex, France

A. D'Onofrio
Università degli Studi di Salerno, Baronisi Salerno, and Istituto Nazionale di Fisica Nucleare, 80125 Napoli, Italy
(Received 21 August 1995)

Evaporation residues (ER) of $Z=34-43$ are measured in singles and in coincidence with emitted protons, deuterons, tritons, and alpha particles. Measurements are done with a large detector array that covers the scattering angles from 2.5° to 25°. The energy centroids of the coincidence spectra of the protons are reasonably well described by statistical model calculations assuming complete fusion, although those for the deuterons and tritons are not. The α-particle spectra are significantly different than the calculated ones. The slopes of the high energy spectra of the protons required a level density parameter $a>A/12$. Comparisons between the experimental ER singles spectra and complete fusion calculations show small deviations that can be explained by incomplete fusion however, when analyzed in coincidence with light particles a very good description with complete fusion is found especially if the emission of intermediate mass fragments is included in the calculations.

PACS number(s): 24.60.Dr, 25.70.Gh

I. INTRODUCTION

The fusion of heavy nuclei has been studied for four decades and has never failed to present us with surprising results every time a new measurement is performed. Recent examples are the energy spectra of light particles [1] and gamma rays [2] and earlier studies of sub- and near-barrier fusion cross sections, which spawned an industry of measurements and theories [3]. All these recurring surprises indicate that fusion of heavy nuclei at energies near and above the Coulomb barrier is still poorly understood and warrants further studies with new or improved techniques.

An important step in understanding fusion and, in general, nuclear collisions at energies near and above 10 MeV/nucleon is the ability to study reaction products by means of exclusive measurements with appropriate gates applied to isolate the various competing reaction mechanisms. Such a study is reported here for products of the reaction ^{79}Br+^{27}Al. Light particles (protons, deuterons, tritons, and alphas) were measured in coincidence with evaporation-residue-(ER-) like fragments of $Z=34-43$ by using the large detector array HILI [4]. With this setup, important questions concerning the emission of light particles from hot compound nuclei can be addressed experimentally. By studying the light particles in coincidence with evaporation residues, no simplifying assumptions concerning the source velocities are needed, and hence characterization of the light-particle spectra in terms of barriers and temperatures becomes meaningful. In addition, by imposing multiplicity cuts on the number of coincident light particles, the isolation of central collisions from more peripheral processes is possible. Since the energies of the residues as well as of the emitted particles are studied in coincidence, issues related to the energy balance in the reaction become accessible to direct study.

Effects such as incomplete momentum transfer will be discussed in the present work, and it will be shown how they can be isolated by adequate triggers. Other aspects to be addressed will be those related to the shape of the energy spectra of the light particles such as deformation of the emitting compound nucleus. Deformation of the emitting compound nucleus has previously been suggested to explain the lower than expected energy where the light-particle spectrum peaks (e.g., Ref. [1]). Another important aspect in the study of the energy spectra of the light particles is the slope of the high-energy part, which can be characterized by the temperature of the emitting system. It has been argued that the unusually high temperatures extracted from particle emission data require level density parameters (a) of the order of $A/12$ [5–7], which are smaller than the common $A/8$ value used at low excitation energies. The detailed analysis of the spectra

*Present address: Argonne National Laboratory, Argonne, IL 60439.

†Present address: University of Maryland, College Park, MD 20742.

 © 1996 The American Physical Society

of the ER is also important in the understanding of the reaction mechanism. It will be shown that the study of the ER spectra in coincidence with the light particles agrees very well with complete fusion predictions especially if the emission of intermediate mass fragments ($Z>3$) (IMF's) is included in the simulations. These questions will be addressed qualitatively as well as quantitatively in this paper through detailed Monte Carlo calculations using a modified version of the code LILITA [8], which is based on the Hauser-Feshbach formulation.

II. EXPERIMENTAL TECHNIQUES

Heavy evaporation residues ($Z\geqslant 34$) of the ^{79}Br+^{27}Al reaction were produced by bombardment of ^{27}Al targets with a 930 MeV ^{79}Br beam obtained from coupled-accelerator operation of HHIRF. The ^{27}Al targets were prepared from foils of high purity aluminum with thickness of 372 μg/cm^2, verified by alpha ranging. Contaminants, mostly oxygen from surface oxidation, were considered to be negligible (below 5%). Coincident light particles were detected with the hodoscope array of the HILI system, which is composed of 192 plastic scintillators that were calibrated with recoil protons produced by an ^{16}O beam on a polypropylene target. The calibration for particles of higher Z and M was done as described in Ref. [4]. Additional checks were carried out by comparing the alpha-particle and $Z=1$ spectra obtained with the hodoscope to those obtained from calibrated Si detector telescopes. For example, the energies measured by hodoscope elements agreed with energies of Si telescopes within 2 MeV for the case of singles α spectra measured for the ^{58}Ni+^{58}Ni reaction at 500 MeV bombarding energy. We estimate the absolute energy calibration to be better than 3%. A typical example of a two-dimensional E-ΔE measured spectrum used for Z identification is shown in Fig. 1. The horizontal axis shows the total E signal of the hodoscope element, and the vertical axis shows the ΔE signal extracted from the 0.5 mm plastic detector placed in front of each hodoscope element. The gates drawn identify very clearly the p, $d+t$, and α+^{3}He particles. The rest of the events are fragments that stop in the ΔE detectors and neutrals (neutrons and γ rays). The hodoscopes alone provide Z identification; the mass of the $Z=1$ and 2 isotopes was determined by time of flight, measured using the cyclotron rf and the time signal of each plastic detector. The yield of the ^{3}He particles was observed to be negligible.

The evaporation residues were measured with the ionization chambers of the HILI system, which were calibrated using the elastic scattering of Br on aluminum and gold. The calibration was extended to lower energies using fragments of Z lower than the beam that penetrated through the ionization chambers and whose maximum energy loss can be determined by using stopping power tables. The major uncertainty in the energy calibration comes from the energy loss corrections that are needed because the fragments lose energy in the entrance parallel plate detector and the entrance foils to the ionization chamber. For example, for the case of 930 MeV ^{79}Br ions, their energy loss before detection predicted by standard stopping power calculation is 90 MeV. Even assuming an uncertainty of 10% in this number, the uncertainty in the total energy will be about 1%. Of course, for lower energies this uncertainty can be bigger.

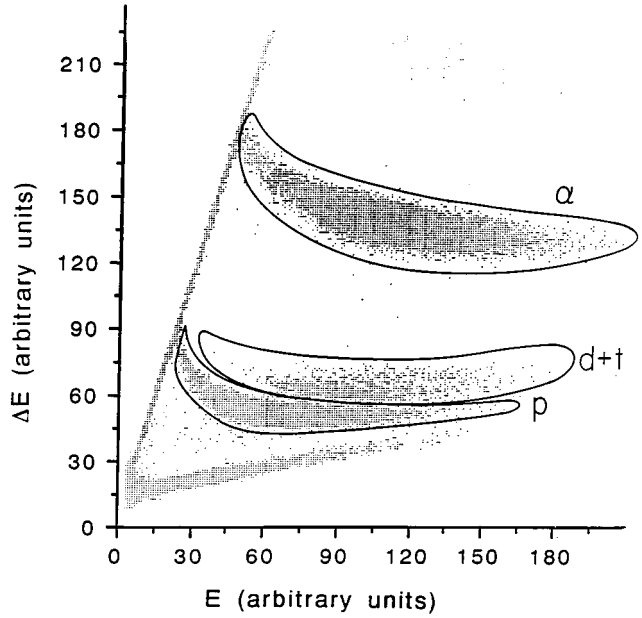

FIG. 1. ΔE vs E array for the light particles emitted in the reaction ^{79}Br+^{27}Al at $E_{^{79}\mathrm{Br}}=930$ MeV. The gates for p, $d+t$, and α are indicated in this figure. The light particles are detected by the plastic elements of the hodoscope of the HILI system.

III. RESULTS: QUALITATIVE FEATURES

Examples of measured energy spectra of evaporation-residue-like fragments ($Z\geqslant 36$) are shown in singles (circles) and in coincidences (crosses) in Fig. 2. The singles spectra were measured in separate runs where events on the ionization chamber were recorded regardless of the status of the hodoscopes. The coincidence requirement, defined as $m=2$, is such that a fragment is considered only if two identified light charged particles (p, d, t, or α) are present in any of the hodoscope's elements. The vertical scale given in the figure corresponds to the actual experimental counts divided by the integrated charge given in μC. The spectra displayed in Fig. 2 are for residues of nuclear charges between 36 and 42 and are given for the whole angular range spanned by the HILI system (2.5°–25°). It should be noted that there is a difference of about a factor of 10 between the singles yield and the $m=2$ coincidence yield. This difference is due to the limited angular coverage of the HILI detector (singles and coincidences should be identical for 4π coverage). A dramatic change is observed between the singles and the $m=2$ spectra. In fact, for the case of $Z=36$, a strong quasielastic component is seen in the singles around an energy of 900 MeV, but disappears completely in the two-particle coincidence case. Also, to a lesser extent the same effect is seen for $Z=38$ ($E\sim 800$ MeV). For higher Z's, like $Z=40$, it is apparent that the shape of the energy spectra does not change with increasing m, which indicates that for these fragments the mechanism is mostly of a central collision nature like complete or incomplete fusion processes. The shift toward lower energy seen in the higher Z spectra may be due to the coincident

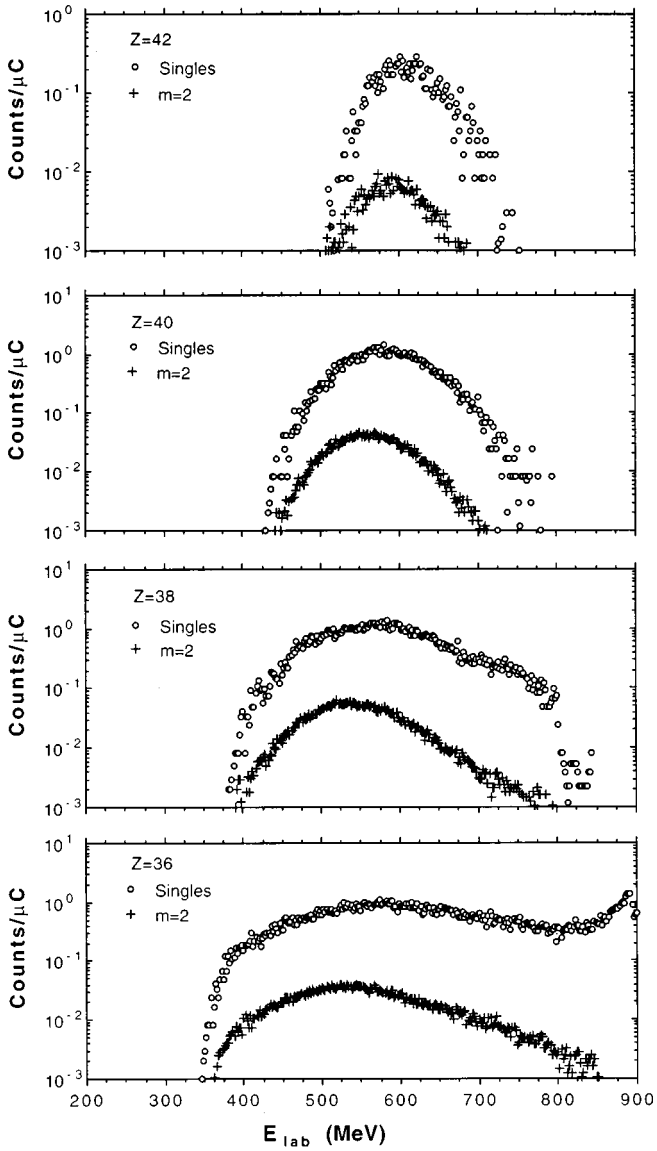

FIG. 2. Experimental spectra for evaporation residues (ER's) of $Z=36-42$ for the reaction 930 MeV $^{79}Br+^{27}Al$. The circles correspond to the singles measurements and the crosses to the requirement that two light charged particles are in coincidence with the ER ($m=2$).

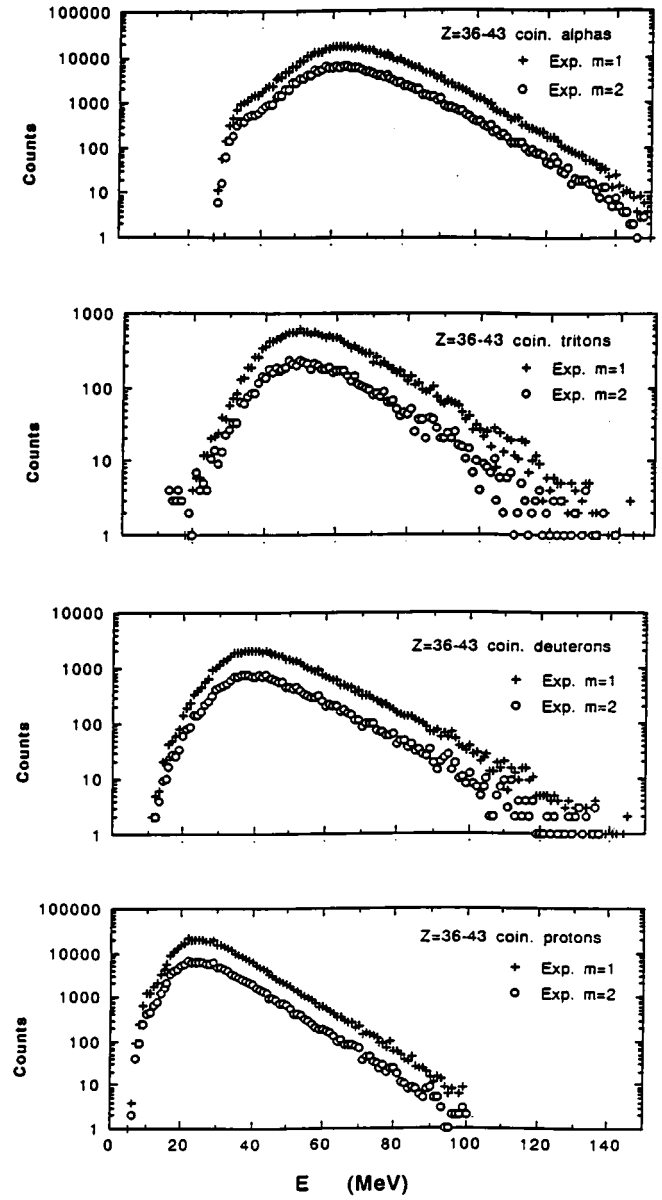

FIG. 3. Experimental energy spectra (circles and crosses) for light charged particles (p, d, t, or α) emitted in coincidence with evaporation residues of $^{79}Br+^{27}Al$ at 11.8 MeV/nucleon. The crosses are for one charged particle in coincidence and the open circles for two (the one indicated in the figure plus any of the four).

constraint which required two light particles to be emitted into forward angles. This bias may depress the efficiency of detecting evaporation residues with higher forward momenta. Our preliminary analysis of these data [9] has already pointed out some of these features.

Energy spectra for p, d, t, and α are shown in Fig. 3. The crosses show data for the case of one light charged particle in coincidence with an evaporation residue ($m=1$), and the open circles show the case of two light charged particles ($m=2$) (one whose spectrum is shown in the figure and an additional identified light charged particle). These spectra were obtained by summing all the counts from each element of the hodoscope for laboratory angles between 2.5° and 25°. The spectra in Fig. 3 have the constraint of being in coincidence with fragments of $Z=36-43$, which were detected with the ionization chamber of the HILI system. The energy cutoffs seen in Fig. 3 (about 8 MeV for p's and 20 MeV for α's) are primarily due to the energy threshold imposed by the 0.5 mm thickness of the ΔE element of the plastic hodoscopes. As can be seen from the data shown in Fig. 3, the spectra have the same shape regardless of the multiplicity requirement, which is in sharp contrast with what is seen in Fig. 2 for the case of the ER's. Further discussions of the features seen in Figs. 2 and 3 will be done in the next section when comparisons to statistical model calculations will be presented.

One unique feature of the present data is that the light charged particles are detected in coincidence, and for every event the velocities of the ER's and coincident light particles are well determined. This allows for the construction of the

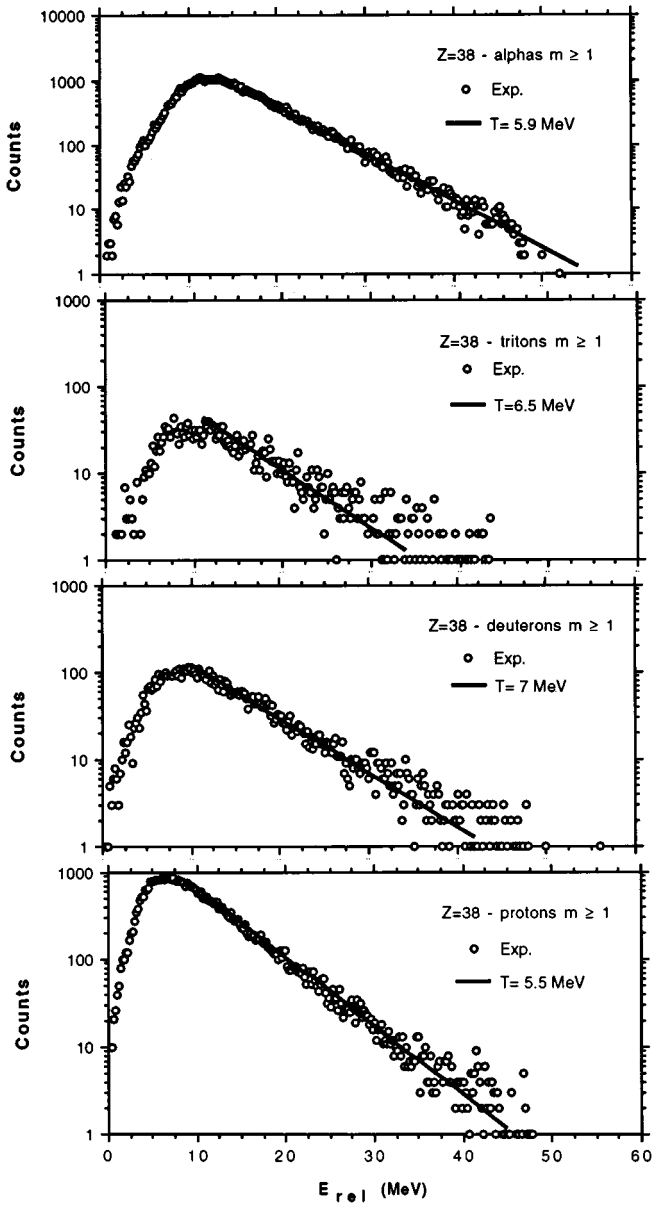

FIG. 4. Spectra of p, d, t, and α particles in coincidence with the ER with $Z=38$ as a function of the relative center-of-mass energy ($E_{\rm rel}$). The experimental spectra are represented by the open circles, and the solid lines are the results of an exponential fit with the indicated slope value T. These spectra were built by determining the relative kinetic energy of each coincident pair in an event-by-event way.

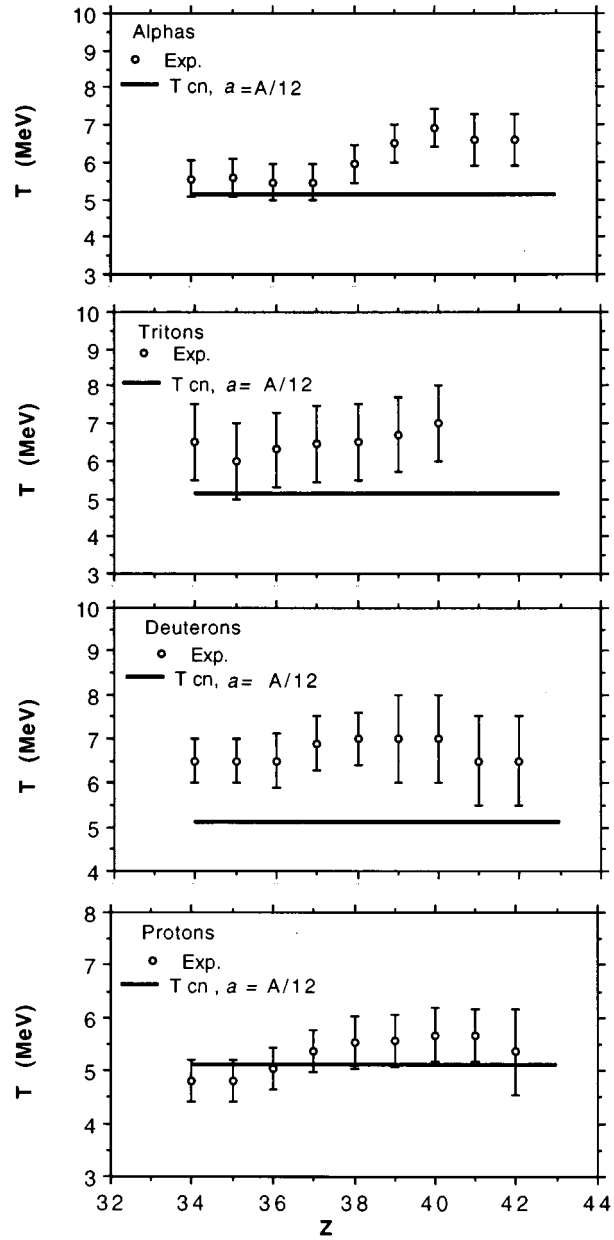

FIG. 5. Temperature parameter (T) as a function of Z of the ER. The T values were deduced from the center-of-mass spectra (like those of Fig. 4) by fitting an exponential to the high-energy slope. The open circles correspond to the experimental values, and the solid lines represent the expected temperature of the compound nucleus for a level density parameter $a=A/12$.

relative kinetic energy spectra ($E_{\rm rel}$) defined by $E_{\rm rel}=(1/2)\mu V_{\rm rel}^2$, where μ is the reduced mass of the pair and $V_{\rm rel}=|V_l-V_{\rm ER}|$ where V_l is the laboratory velocity of the light particle and $V_{\rm ER}$ that of the ER. The mass of the ER (our experiment measures only Z) was estimated by assuming that the most probable mass of each residue will have the same neutron to proton ratio as the projectile ^{79}Br.

The results for $E_{\rm rel}$ are shown in Fig. 4 for the $m\geqslant 1$ case (open circles) for the p, d, t, and α in coincidence with residues of $Z=38$. These spectra will be used to extract the slope parameters (T) from the high-energy part of the spectra. These slope parameters can be related to the nuclear temperature and are extracted by fitting the expression $\exp(-E_{\rm rel}/T)$ to the high-energy part of the spectra. The solid lines drawn in the figure correspond to the best fit for the indicated T value. The values of T extracted from the experimental spectra for every light particle in coincidence with the ER are shown in Fig. 5. The solid line corresponds to the expected temperature for the compound nucleus formed in this reaction (5.1 MeV) obtained by using the level density parameter $a=A/12$, which is consistent with current systematics [5–7], and assuming a maximum excitation energy of 230 MeV, which corresponds to the complete fusion value. Although the error bars are substantial, a few trends do emerge from the data shown in Fig. 5. In the cases of p and

α particle emission, the extracted temperatures increase with the mass (charge) of the heavy fragment in coincidence. This variation is probably due to the experimental bias introduced by the gating on the final product in the cascade. To reach lower masses, smaller amounts of energy have to be removed during each evaporation (on average); therefore, gating on lighter products emphasizes cascades where the emitted particles removed less energy, i.e., had less kinetic energy. The d and t emissions are only a small part of the cascade and have minimal effects on the energy balance throughout the cascade. The average value of T extracted over all the Z values for p, d, t, and α are (in MeV) 5.3, 6.7, 6.5, and 6.0, respectively, with the d and t showing the largest values, maybe due to their propensity to be emitted early in the cascade. One important feature of the experimental T values shown in Fig. 5 is that they all lie above 5.1 MeV, which is the expected temperature extracted with a level density parameter value of $A/12$. This in support of the idea [6,7] that for high excitation energies the level density parameter (a) should decrease significantly from its low excitation value of $A/8$. The relationship between the slope and temperature of the emitting system is only an approximation. The sampling of the particles spectra harbors in it, not only the fluctuation due to the particle emission, but also the uncertainty in the source velocity that contributed to the yields seen at low energies (below the Coulomb barrier) and increases the high energy slope by about 10%–20%. More discussions of these subjects will be given in the next section where the statistical model calculations are presented.

IV. ANALYSIS: QUANTITATIVE

A. Complete fusion

Since most of the light particles are in coincidence with heavy fragments which have Z's characteristic of ER of the compound nucleus, the experimental results can be compared to Hauser-Feshbach calculations assuming that the particles are emitted by a compound nucleus formed at equilibrium following a complete fusion (CF) reaction. Hauser-Feshbach calculations were performed using the Monte Carlo code LILITA [8]. Substantial modifications were made to the code to improve the statistical model calculations. The most important one was the introduction of transmission coefficients obtained with an optical model calculation using the optical model parameters of Ref. [10]. (The original version of LILITA has a simple parametrization for low excitation energies plus a sharp cutoff for high excitation energies.) The calculations were done using the value of $A/8$ for the level density parameter (standard value used at low excitation energies) and the dependence of deformation on angular momentum described by Huizenga *et al.* [11]. For the ^{79}Br+^{27}Al fusion reaction, a critical angular momentum of $75\hbar$ was used, consistent with previous analysis of fusion cross sections [12,13] of similar mass numbers for target plus projectile. Small changes, on the order of 10%, to the value of the critical angular momentum have negligible effects on the comparisons, which will be shown. The calculations are of the Monte Carlo type and therefore are done in an event-by-event manner, trying to simulate as much as possible the experimental condition. Therefore, the same experimental constraints of geometry, thresholds, energy losses in foils, etc., placed by the HILI system on the experimental spectra have been applied to the calculations.

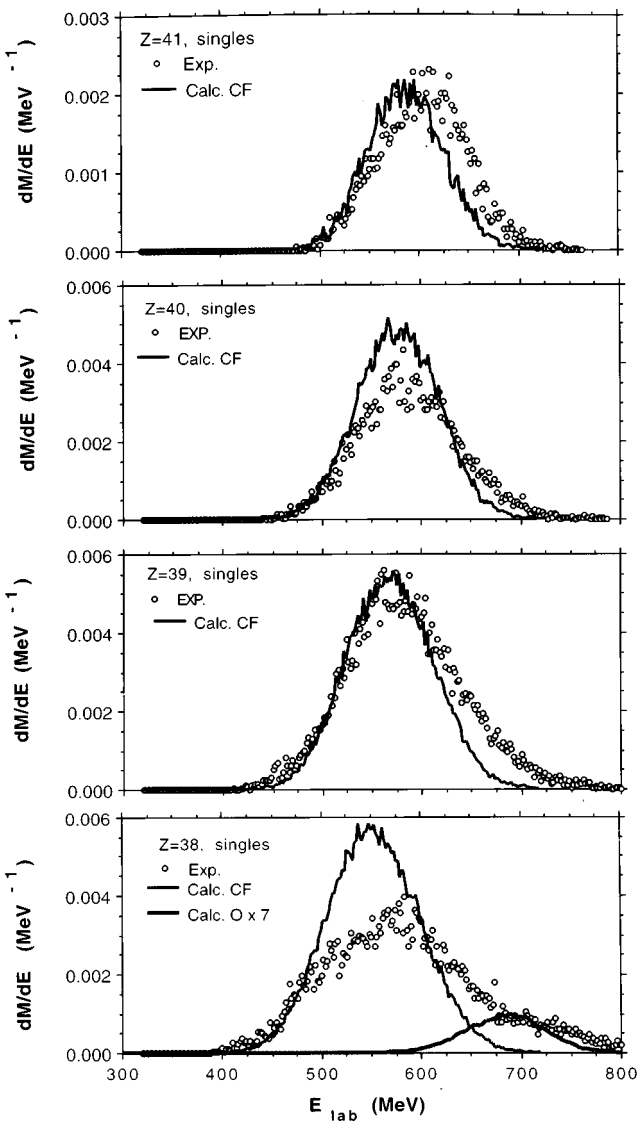

FIG. 6. Singles spectra of fragments of $Z=38-40$. The solid lines are the results of a complete fusion calculation. The vertical axis (differential multiplicity) is explained in the text. The thick solid line (labeled O×7) drawn for $Z=38$ corresponds to the simulation of the oxygen contaminant in the target.

The first important comparison to do between the experimental spectra and calculations is for the singles yields of ER's. Figure 6 shows such a comparison for the energy spectra of residues of $Z=38$, 39, 40, and 41. The spectra have been integrated over all the angular coverage of the HILI detector. The solid lines are the Monte Carlo prediction, which assumes CF and equilibrium decay. Plotted on the vertical axis is the differential multiplicity (dM/dE) defined as the ratio of the counts of a given residue in the energy bin dE (1 MeV steps) to the total residue counts (integrated over angle, energy, and Z for $Z\geqslant 38$). Several features are important to discuss from the comparisons shown in Fig. 6. The most obvious one is the general agreement of the magnitude of the differential multiplicities except for $Z=38$, which is overpredicted by about a factor of 2. The calculations predict

reasonably well the decrease in multiplicities from $Z=39$ (maximum about 0.005) to $Z=41$ (maximum about 0.002). In addition, for $Z=39$ and 40 the centroids of the experimental energy spectra are well reproduced by the calculation. Two discrepancies stand out in the comparisons shown in Fig. 6: The widths of the calculated spectra are slightly narrower, and the centroids for the calculated spectra, especially for $Z=38$ and 41, are shifted towards lower energies. The shift in the energy spectrum for $Z=41$ can be understood in the context of a simple incomplete fusion (IF) mechanism. According to Refs. [14–16], the most likely IF process is to lose particles from the lighter of the two partners in the reaction (^{27}Al in this case). Such an IF process will predict spectra with more events at higher energies, which is what is seen in Fig. 6 for $Z=41$. The discrepancy in the centroids of experimental and calculated spectra for $Z=38$ is more likely to arise from the fact that for $Z=38$ other more peripheral processes can be present. More details on these effects will be given later on when the energy spectra of the residues in coincidence with the emitted light particles will be presented.

It was mentioned in Sec. II that the Al target had less than 5% of oxygen contamination. Before continuing with the analysis of the ^{79}Br+^{27}Al data, it is important to assess the possible contributions to the residue energy spectra of this contaminant. The fusion of ^{79}Br+^{16}O will produce ER's of similar Z ($\sim$38) as those of the ^{79}Br+^{27}Al reaction, although with much less intensity and with a more forward peak angular distribution due to the very light mass of the target (^{16}O), making the effect even less important due to the 3° opening of the HILI detector. Nevertheless, it is important to establish the relevance of this contamination. The best way is to simulate, in the same manner as was done for the ^{79}Br+^{27}Al reaction (results shown in Fig. 6), the ^{79}Br+^{16}O fusion. The simulations were also done with the code LILITA using a set of statistical model parameters consistent with the one used for the Al target. The result of the calculation for the energy spectra of residues of $Z=38$ is shown by the thick solid line on the bottom panel of Fig. 6. The calculation has been renormalized by a factor of 7, and so it can be plotted in the figure. As can be seen, the predicted centroid of about 700 MeV could overlap with the peripheral component of the Br+Al reaction. However, the expected yield is very small and can certainly be neglected. We chose to compare to the $Z=38$ spectra because the calculation predicted the maximum cross section for this Z for the fusion of ^{79}Br+^{16}O. (To show also that the oxygen contaminant is negligible in the analysis of the light particles in coincidence with the ER, we have added on the bottom panel of Fig. 10 the effect of the oxygen contamination on the α-particle spectra in coincidence with $Z=38$.)

Comparisons between the experimental and calculated energy spectra (integrated over the angular coverage of the HILI detector) of the emitted p, d, t, and α's are shown in Figs. 7–10 where the open circles represent the experimental values and the crosses the calculations. The vertical scale refers to the differential multiplicity dM/dE defined as the number of light particles in a given energy bin dE divided by the number of residues of charge Z, indicated in the figure. The spectra shown in Figs. 7–10 were taken in coincidence with a given evaporation residue with the additional constraint that at least one charged particle be in coincidence (total multiplicity in the detector $m\geqslant 1$). Residues of $Z=38$–40 were chosen for the comparisons in Figs. 7–10 because they are the most probable fragments that are produced in a complete fusion reaction. The first observation to be noticed from the comparisons shown in Figs. 7–10 is that the maximum of the differential multiplicities is only reasonably well predicted for the proton case (Fig. 7). The maxima for the deuterons are overpredicted by about a factor of 3 and for the tritons by a factor of 4. For the α-particle case (Fig. 10), the high-energy multiplicity is well predicted, but the maximum is shifted with respect to the experimental spectrum. More discussions on the yields of the light particles in coincidence with the ER will be given later after commenting on the shape of the energy spectra.

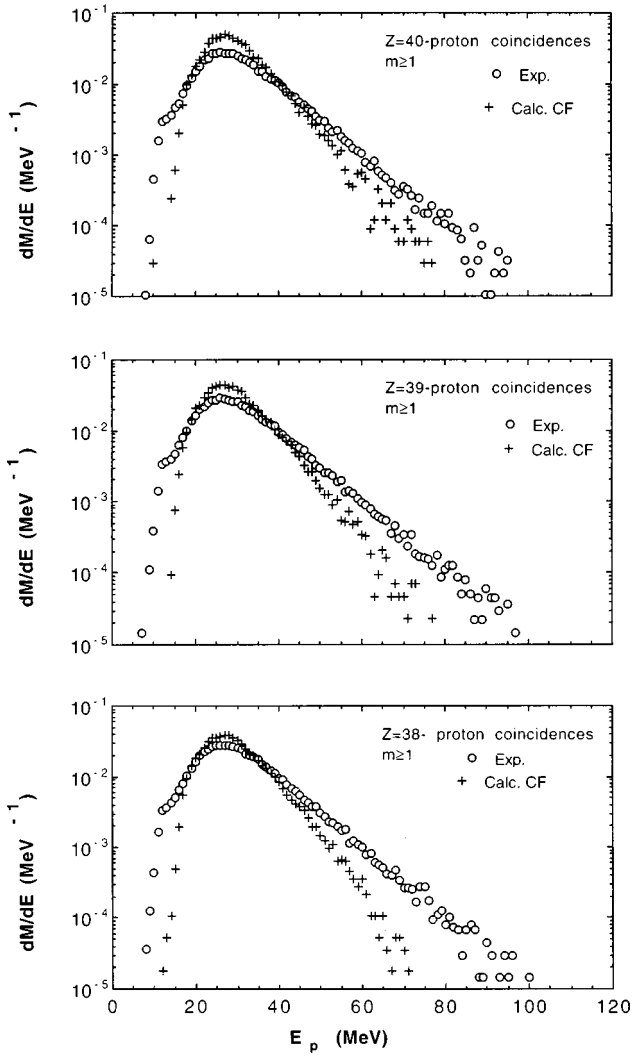

FIG. 7. Experimental energy spectra (circles) for any proton in coincidence with ER's of $Z=38$, 39, and 40. The statistical model calculations for complete fusion are given by the crosses. The vertical axis (differential multiplicity) is explained in the text.

The comparison between the data (open circles) and calculations (crosses) shown in Fig. 7 for p's in coincidence with the specified residues indicate that the data are certainly consistent with emission from a compound nucleus. A slight deviation is seen for energies above 50 MeV where the cal-

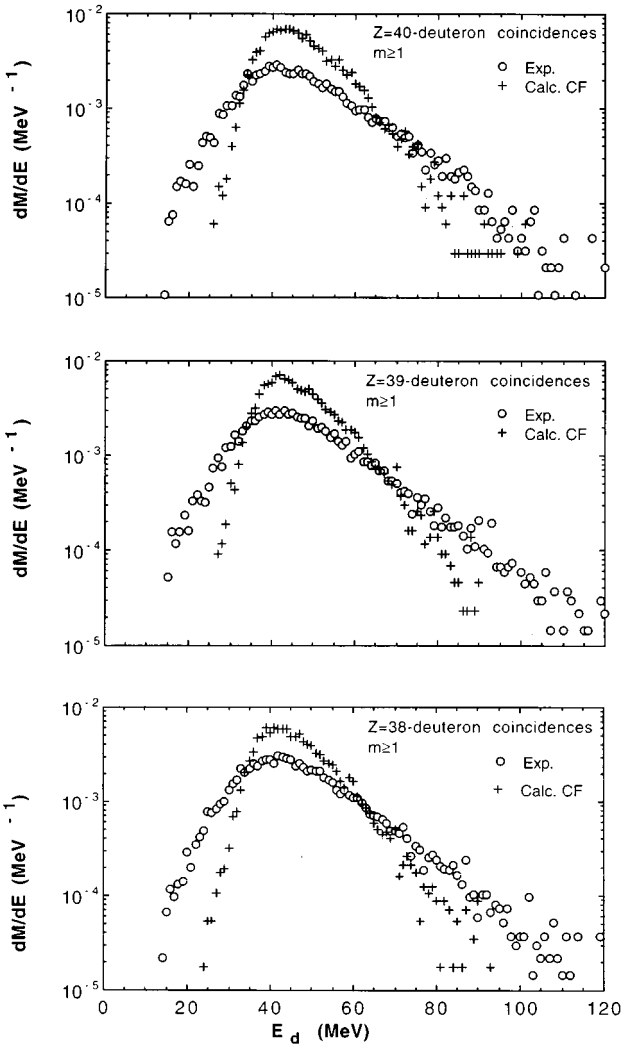

FIG. 8. Experimental energy spectra (circles) for any deuteron in coincidence with ER's of $Z=38$, 39, and 40. The statistical model calculations are given by the crosses. The vertical axis (differential multiplicity) is explained in the text.

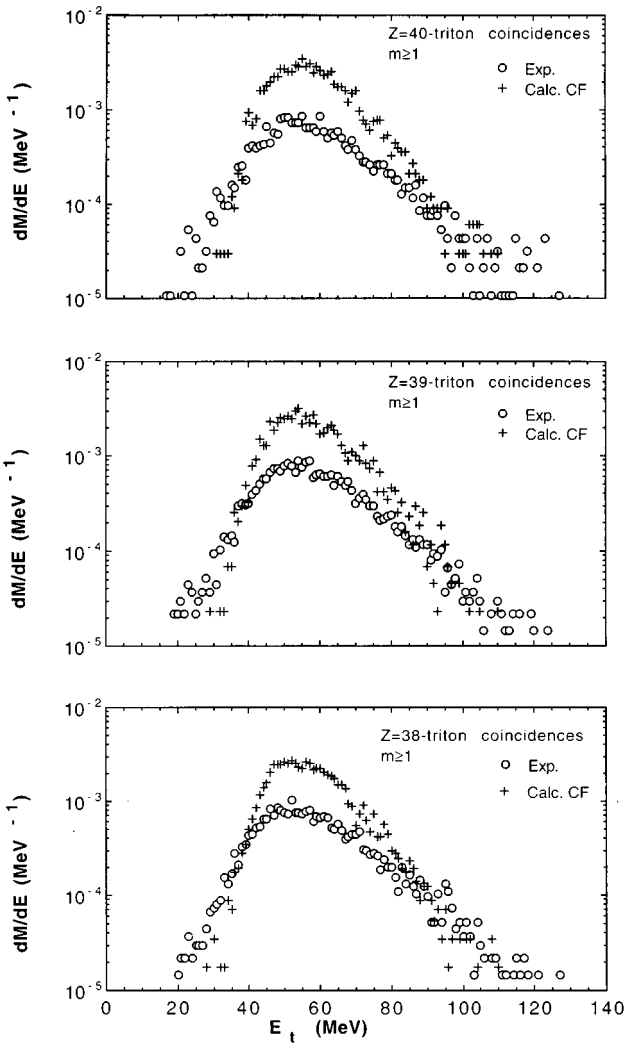

FIG. 9. Experimental energy spectra (circles) for any triton in coincidence with ER's of $Z=38$, 39, and 40. The statistical model calculations are given by the crosses. The vertical axis (differential multiplicity) is explained in the text.

culation falls off more rapidly than the data. Although the high-energy behavior of the calculated spectra depends strongly on the level density parameter a, it will be shown later that the use of surface absorption in the optical model potential parameters, employed to calculate the transmission coefficients, also has a sizable effect. A small shift can be seen on the low-energy side of approximately 1 MeV: its possible interpretation could be related to deformations of the compound nucleus of the kind discussed in Ref. [1].

Depicted in Fig. 8 are the experimental (open points) and calculated (crosses) spectra for the case of deuterons in coincidence with residues of $Z=38-40$. A significant discrepancy between prediction and data can be noticed already. The low-energy part is not well reproduced, and the widths of the predicted spectra are narrower than those of the data. Previous experiments have not observed such large differences, although in the work reported in Ref. [17] it is pointed out that the difference in the yield of deuterons between standard statistical model calculations and data may be due to the choice of transmission coefficients and level density parameters. The high-energy behavior is similar to the proton spectra. For the emitted tritons in coincidence with ER's (Fig. 9), the agreement between data and calculations is slightly better than for the deuteron case; both the low-energy part of the spectra and the width are reasonably well reproduced, and only small deviations are seen. The high-energy behavior is reproduced much better than for p's and d's.

From Fig. 10, which compares data and predictions of α spectra in coincidence with residues, it is obvious that a very large shift of about 10 MeV is seen in the low-energy part of the spectra. This shift is so large that if it were interpreted in terms of static deformations the deformation would have to be very large, i.e., an equivalent reduced radius of $\sim$2.3 fm. Similar shifts in α-particle spectra have been reported in Ref. [18] for a compound system of slightly heavier mass than the one discussed here. It is important to emphasize that using a different level density parameters will not change appreciably the low-energy shape of the predicted α spectra shown in Fig. 10. Most of the changes will occur at the high-energy end of the spectra. In the work of Ref. [18], dynamical effects are called for to explain the anomalous low-energy α

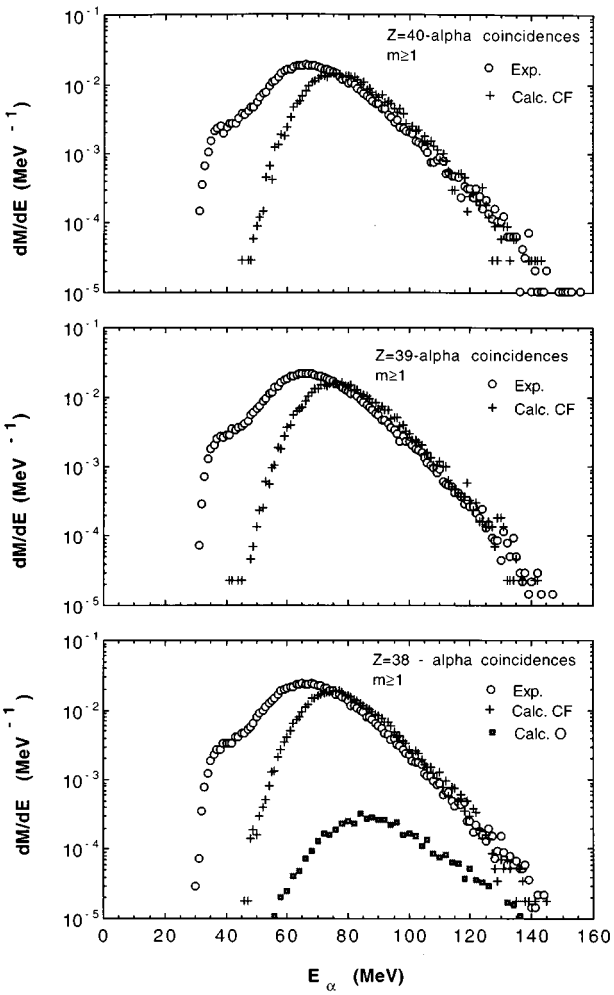

FIG. 10. Experimental energy spectra (circles) for any α in coincidence with ER's of $Z=38$, 39, and 40. The statistical model calculations are given by the crosses. The vertical axis (differential multiplicity) is explained in the text. The squares (labeled O) correspond to the calculated α spectra expected from the oxygen contaminant in the target.

emission. In the present work, we propose that the most likely effect for the discrepancies seen in Fig. 10 is of a dynamical nature like preequilibrium shape emission or incomplete fusion.

As mentioned earlier, one can see from Figs. 7–10 that the magnitudes of the predicted differential multiplicities (dM/dE) are not in good agreement with the experimental ones. One way to further illustrate this point is to analyze the integrated multiplicity M, obtained by integrating over energy the differential multiplicities. In Fig. 11, we show the experimental multiplicities M for emission of p, d, t, and α as a function of the Z of the residue. To minimize effects due to reactions other than fusion, the additional constraint of requiring that more than one light charged particle be detected has been applied. This means that at least a triple coincidence requirement is fulfilled (one residue, the indicated light particle, plus one more light charged particle). It should also be kept in mind that the fragments of $Z=34$ and 35 may have large nonfusionlike components. The calculated multiplicities M are shown as lines in Fig. 11. The main

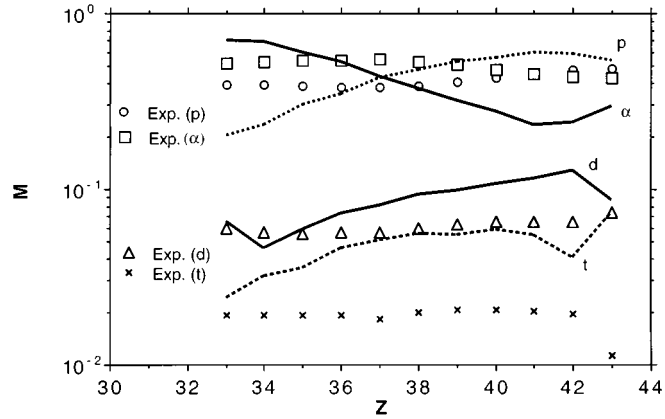

FIG. 11. Integrated multiplicity M of p (circles), d (triangles), t (crosses), and α (squares) as a function of the Z of the ER. The lines (solid and dashed) correspond to the calculated values assuming a complete fusion mechanism with a level density parameter of $A/8$. The coincidence requirement is $m\geqslant 2$.

observation to make from Fig. 11 is that the calculated M for tritons overpredicts the experimental one by about a factor of 3 almost independently of Z, although it should be noted that the overall probability of emission of a triton is very small. The difficulties in predicting the yields of triton have been pointed out previously in Ref. [17]. The predicted probabilities for p, d, and α as a function of Z are all better than a factor of 2, although it is evident that the calculated α multiplicities are low and the proton multiplicities are high for $Z>38$. From the comparisons shown in Figs. 10 and 11, it is already evident that mechanisms other than complete fusion should be explored.

We next examine the energy spectra of the heavy residues in coincidence with light particles: The calculated spectra for the residues of $Z=38$, 39, 40, and 41 (solid lines) are shown in Fig. 12. The calculations are part of the same simulation used to generate the light-particle spectra shown in Figs. 7–10. The coincidence requirement for these spectra ($m\geqslant 1$) is that at least one charged particle (p, d, t, or α) be registered with the residue. The conclusions that can be drawn from the comparisons shown in Fig. 12 are entirely similar to the ones discussed already for the singles spectra shown in Fig. 6. The agreement between experiment and calculations is better for $Z=38$ and 39 than in Fig. 6 mainly because the coincidence requirement reduces the events in the high-energy portion of the experimental spectra. Even in coincidence there is still a disagreement on the high-energy portion of the spectra, in particular for $Z=41$, and also the predicted spectra are narrower than the experimental ones. This together with the discrepancies discussed earlier in connection with the light-particle spectra (Figs. 7–10) indicates that other mechanisms like incomplete fusion should be considered and that is done later on.

B. Complete fusion calculation and uncertainties in the level density

The calculations presented in Sec. IV A were done using the standard level density parameter of $a=A/8$; however, recent analyses have suggested smaller values, like $A/10$, or even that an energy-dependent level density parameter

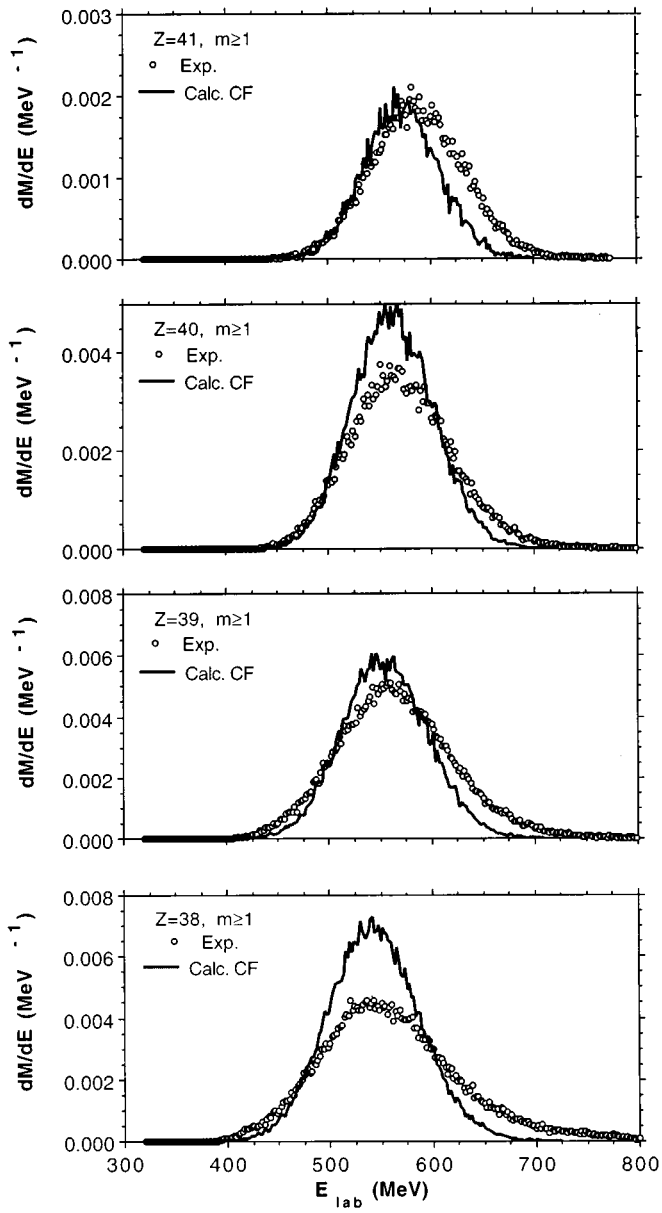

FIG. 12. Experimental energy spectra (circles) of ER's of $Z=38-41$ in coincidence with any light charged particle ($m\geqslant 1$) p, d, t, or α. The solid lines are the statistical model calculations for complete fusion. The differential multiplicity given in the vertical axis is explained in the text.

should be used [6,7]. Also, in connection with the analysis of the data given in Fig. 5, a value of $A/12$ could be more appropriate. To investigate to what extent the discrepancies between the data and calculations are due to uncertainties on the level density, a full set of simulations was done using the level density parameter of $A/12$.

The first comparisons of interest to discuss are on the energy spectra of the light particles emitted in coincidence with the ER. Figure 13 shows these spectra for p and d in coincidence with $Z=38$, and Fig. 14 shows t and α in coincidence also with $Z=38$. The vertical scale in Figs. 13 and 14 gives the differential multiplicity dM/dE, as defined earlier in connection with Figs. 7–10. Comparing the p spectra with the corresponding one for the $A/8$ calculations (bottom

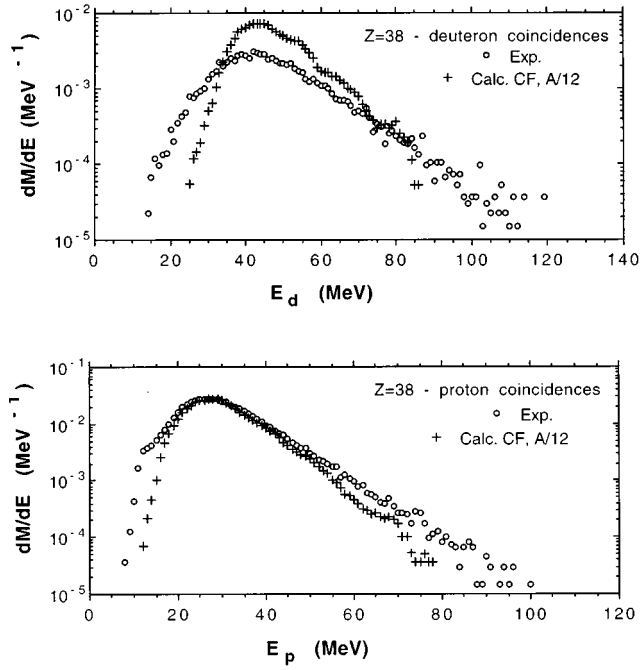

FIG. 13. Experimental energy spectra (circles) for protons (bottom panel) and deuterons (top panel) in coincidence with $Z=38$. The calculations (crosses) are for a complete fusion process calculated with a level density parameter of $a=A/12$.

panel of Fig. 7), a much better fit to the experiment can be seen by using $A/12$. The magnitude of the maximum of the spectra is well reproduced as well as the high-energy behavior (although still the predicted spectra falls off faster than

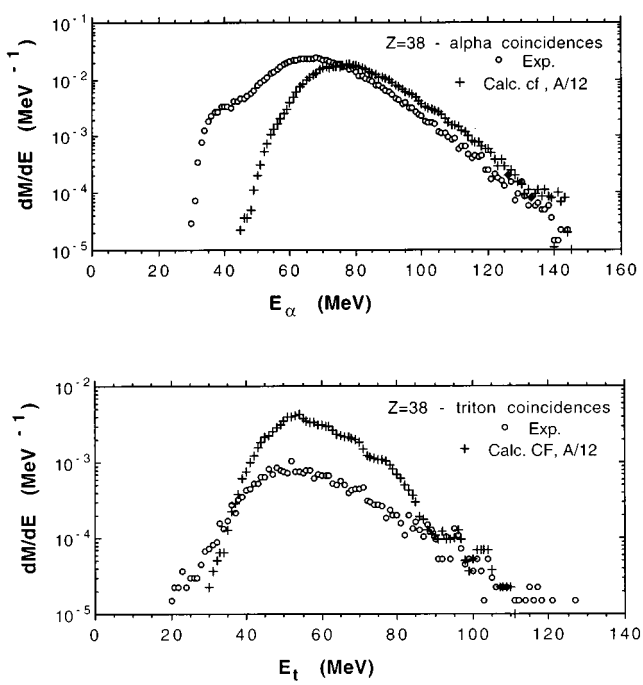

FIG. 14. Experimental energy spectra (circles) for tritons (bottom panel) and α's (top panel) in coincidence with $Z=38$. The calculations (crosses) are for a complete fusion process calculated with a level density parameter of $a=A/12$.

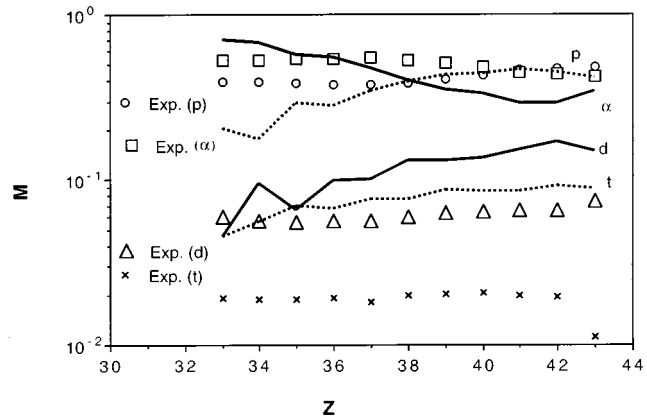

FIG. 15. Integrated multiplicity M of p (circles), d (triangles), t (crosses), and α (squares) as a function of the Z of the ER. The lines (solid and dashed) correspond to the calculated values assuming a complete fusion mechanism with a level density parameter $a=A/12$. The coincident requirement is $m\geqslant 2$.

the data). For the d case, top panel of Fig. 13 and bottom panel of Fig. 8, it can be seen that the high-energy behavior of the calculated spectrum improves as compared to the experiment. The comparisons for the t and α spectra (Fig. 14 and bottom panels of Figs. 9 and 10) do not clearly indicate a preference between $A/8$ or $A/12$. Although the observations made on the data given in Figs. 13 and 14 are based on the analysis of the light charged particle spectra in coincidence with $Z=38$, they remain the same by analyzing the other Z's from 39 to 41.

Another useful comparison is of the energy-integrated multiplicities M, similar to those shown in Fig. 11 for the $A/8$ case. The results using the level density of $A/12$ are shown in Fig. 15. The main observation is that for $Z>37$ (the relevant region for complete fusion) the agreement within the experimental (squares) and calculated (dashed lines) M values for p is very well reproduced. For the α-particle case, the predictions (solid lines) are slightly better than in Fig. 11. The multiplicities for d and t are not well predicted just as in Fig. 11. From the comparison shown in Figs. 7–11 and 13–15 and based on the high-energy slopes of the p and d spectra, it can be concluded that a slightly better description of the data can be achieved by using the value of $A/12$, supporting the idea [6,7] that for higher excitation energies (like in this case about 180 MeV) a lower value of the a parameter should be used. The calculations for the energy spectra of the ER like those shown in Fig. 6 were done for the $A/12$ case, but no significant change was seen and, therefore, they are not shown. Also, it is important to notice that the uncertainties in level density do not explain the anomalous low-energy α emission, and therefore further explanations have to be found.

C. Incomplete fusion processes

From the comparisons shown in Figs. 6 and 12, it is clear that the process of complete fusion does not fully explain the data, which suggests that an additional component is needed to explain the discrepancy particularly in the $Z=41$ spectra. A typical mechanism is that of IF as discussed in Refs. [14–16]. Following IF systematics [14–16], a 10% contribution of IF with particles lost from the lighter of the two partners (the target in this case) should be expected. A complete simulation was done using a 10% contribution of IF, but no effect was clearly seen with respect to the complete fusion calculations; therefore, a 20% component had to be assumed in order to have sizable effects. These simulations assumed a loss of an α particle from the target with a complete fusion of the projectile with the target remnant (^{23}Na) at a projectile energy of 11.8 MeV/nucleon. The critical angular momentum used was $70\hbar$, five units less than the complete fusion case essentially due to the mass loss. All simulations were done using the standard level density $A/8$.

The first result of the IF calculations that we want to discuss is for the residue energy spectra, which are shown in Fig. 16, for fragments of $Z=38-41$ in coincidence with any light charged particle. The data (open circles) are the same as presented in Fig. 12. As can be seen from the comparisons, the centroid for the spectra for $Z=41$ is much better predicted for the CF+IF calculation than for the CF alone (Fig. 12). In general, the shapes of the spectra for $Z=38-40$ are as well reproduced or better than for the CF case. The overprediction of the magnitude of the differential multiplicity for $Z=38$ (same as in Fig. 12) and the fact that the predicted widths of the spectra are significantly narrower than the data indicate that although an IF process may be present still other effects could be important. The next important result to present in the IF calculations is in the energy spectra of the p, d, t, and α emitted in coincidence with the ER. In Fig. 17 we show the results for the p and d in coincidence with $Z=38$ and in Fig. 18 those for t and α also in coincidence with $Z=38$. The data (solid points) are the same as those of Figs. 13 and 14. The results of the CF+IF calculations (crosses) shown in Figs. 17 and 18 compared to the calculations given in Figs. 13, 14, and 7–10 are very similar, which means that the major discrepancies between the experimental spectra and the calculations are not due to an incomplete fusion mechanism and, therefore, still other processes will have to be considered. In particular, it should be noted that the calculated spectra for α's in coincidence with $Z=38$ (Fig. 18) show still the large discrepancy with the data at low energies (also seen in Fig. 10).

D. Influence of other decay channels in complete and incomplete fusion calculations

So far, the calculations given in Secs. IV A, IV B, and IV C contain five decay channels n, p, d, t, and α, and hence uncertainties can be introduced if not all the important channels are included. Recently, in the study of the Kr+Al reaction at 10 MeV/nucleon [19], large cross sections have been reported for decay of binary channels when one of the reaction partners has a $Z>2$. Also earlier work [20] in the study of the ^{58}Ni+^{58}Ni at 11 MeV/nucleon, large cross sections for the emission of intermediate mass fragments ($Z\geqslant 3$) (IMF's) have been reported. Following the analysis done in Ref. [20], we have calculated the first step emission of the deexcitation process using the code BUSCO [20], which uses many emission channels up to $Z=20$. The output of this calculation is fed into the full Monte Carlo deexcitation process with the code LILITA, but for the multiple steps using only the five light-particle channels (n, p, d, t, and α). The statistical

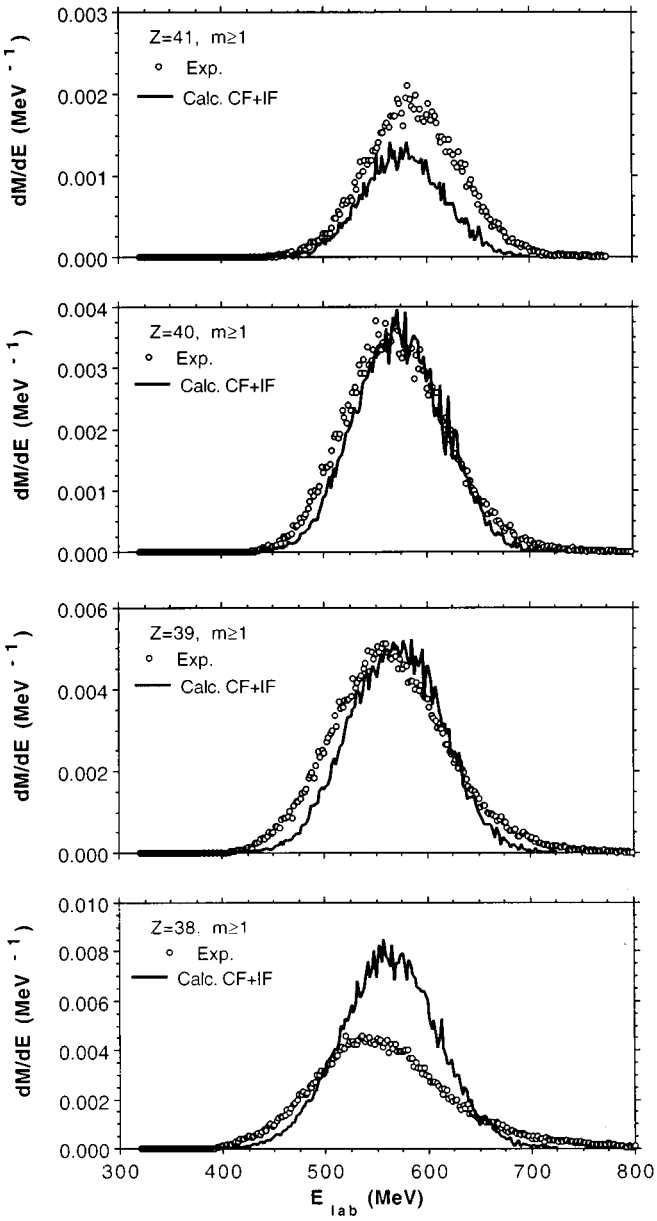

FIG. 16. Experimental energy spectra (circles) of ER's of $Z=38-41$ in coincidence with any light charged particle ($m\geqslant 1$) p, d, t, or α. The solid lines are the statistical model calculations for complete fusion plus 20% of incomplete fusion contribution. The differential multiplicity given in the vertical axis is explained in the text.

model parameters are the same as used in Sec. IV A. The first results of these many channels calculations are shown in Fig. 19 for the case of evaporation residues in coincidence with one or more light charged particles. The data are the same as those given in Figs. 6 and 16. The most important result of the comparisons shown in Fig. 19 is that the width of the predicted residue spectra is now in very good agreement with the experiment, although there are still problems with the absolute prediction of the values of the differential multiplicities. The shift seen for the case of $Z=41$ is due to the fact that the calculations in Fig. 19 have only the complete fusion component. Another important result of these calculations will be the comparisons with the energy spectra

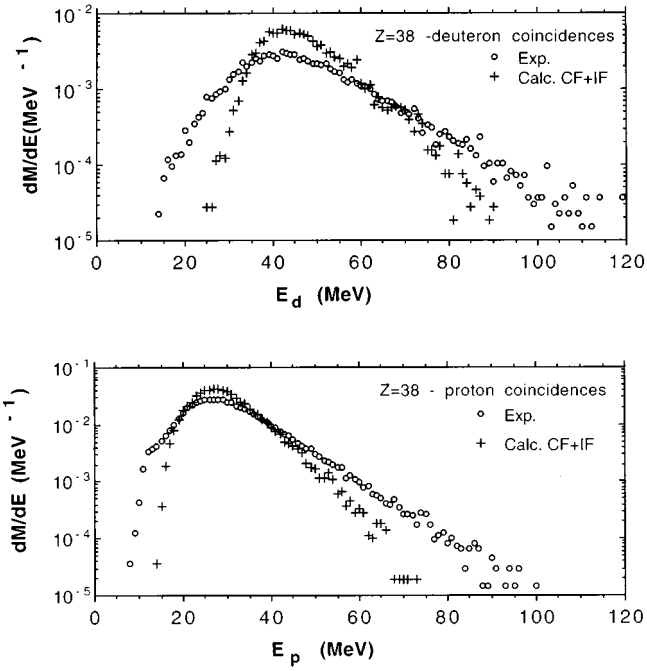

FIG. 17. Experimental energy spectra (circles) for protons (bottom panel) and deuterons (top panel) in coincidence with $Z=38$. The calculations (crosses) are for a complete fusion process plus a 20% contribution of incomplete fusion.

of the emitted light particles. The results for the spectra of p and d in coincidence with $Z=38$ are shown in Fig. 20, and those for t and α also in coincidence with $Z=38$ are shown in Fig. 21. The results shown in Figs. 20 and 21 have to be

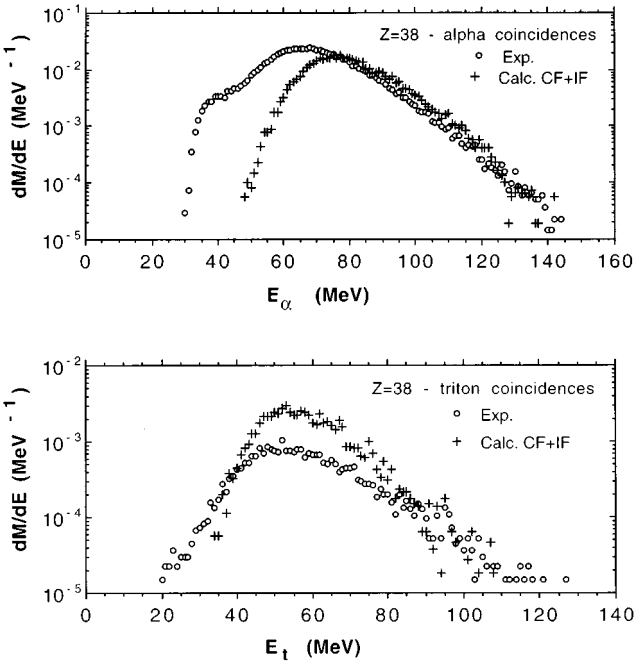

FIG. 18. Experimental energy spectra (circles) for tritons (bottom panel) and α's (top panel) in coincidence with $Z=38$. The calculations (crosses) are for a complete fusion process plus a 20% contribution of incomplete fusion.

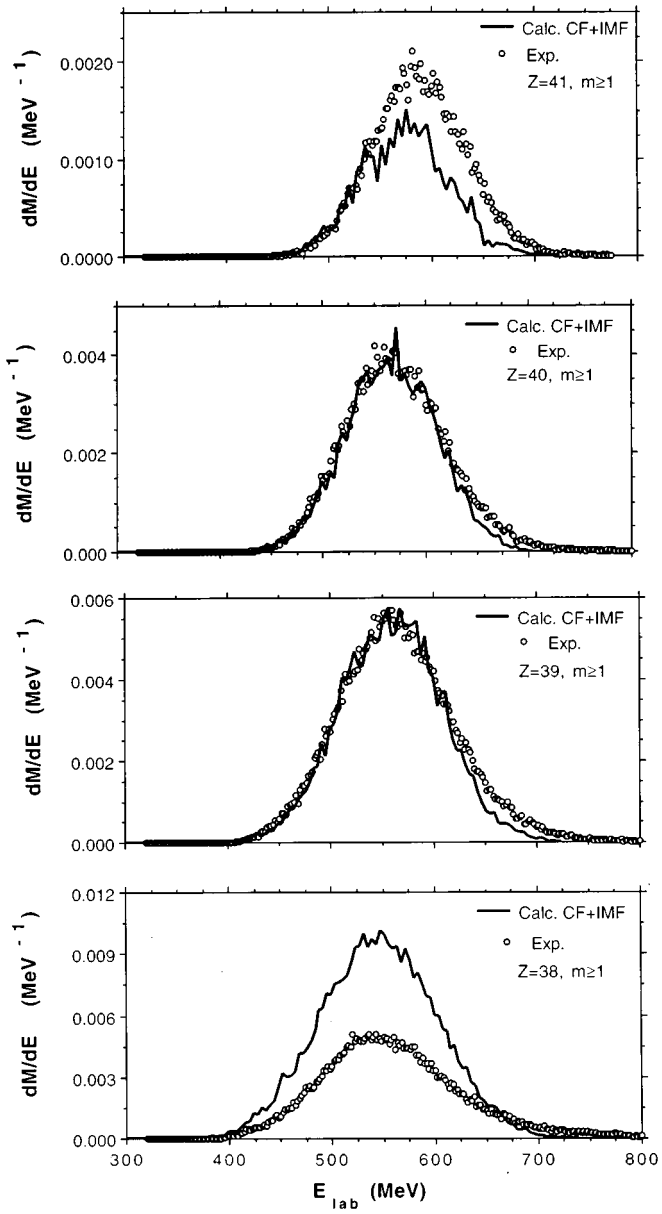

FIG. 19. Experimental energy spectra (circles) of ER's of $Z=38-41$ in coincidence with any charged particle ($m\geqslant 1$) p, d, t, or α. The solid lines are the statistical model calculations for complete fusion assuming all decay channels (mainly light particles and IMF's up to $Z=20$). The differential multiplicity given in the vertical axis is explained in the text.

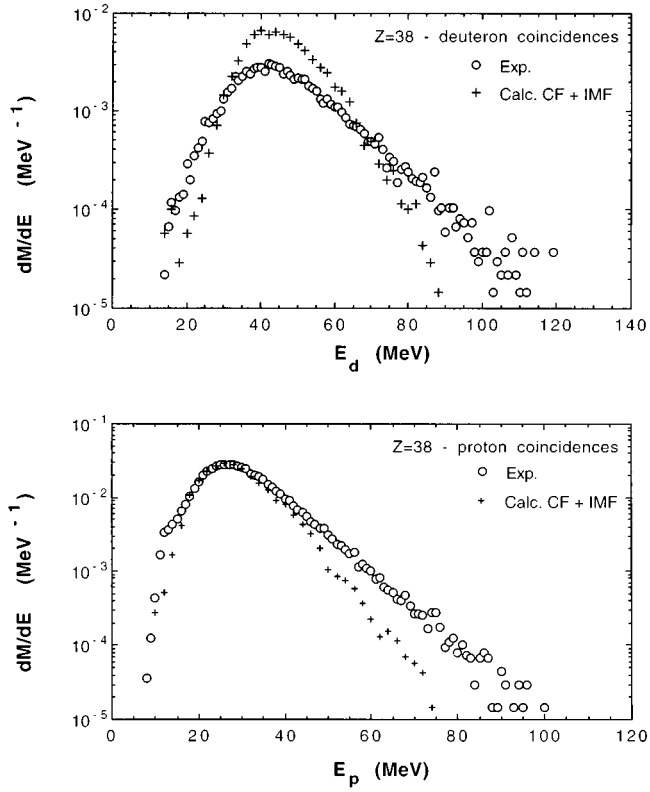

FIG. 20. Experimental energy spectra (circles) for protons (bottom panel) and deuterons (top panel) in coincidence with $Z=38$. The calculations (crosses) are for a complete fusion process assuming all decay channels (mainly light particles and IMF's up to $Z=20$).

compared to the CF+IF case (Figs. 17, 18) and with the CF case (Figs. 7–10). A significant improvement can be seen for all the spectra shown in Figs. 20 and 21 with respect to the other calculations, implying that a full deexcitation mechanism including IMF's is important to improve the prediction of the complete fusion mechanism. However, even if significant improvement is seen, still the excess of low-energy counts in the α spectra is evident (see Figs. 10, 18, and 21). Clearly, other mechanisms not considered so far should be responsible for the emission of low-energy α particles.

E. Processes other than CF or IF

The most important difference between the experimental data and all the calculations presented so far is in the low-energy part of the α spectra. One mechanism that has been mentioned earlier that could account for such low-energy α's is the deformation effects in the compound nucleus. A simple estimation of the amounts that the barrier must decrease in order to fit the data gives a radius parameter of about 2.3 fm, a very large radius indeed (10.9 fm for a ^{106}Cd nucleus). However, perhaps more plausible mechanisms can be invoked to explain this anomaly. One such mechanism is that of preequilibrium shape emission. Indeed, it is possible that emission could occur with the system formed in an intermediate state of a dinuclear shape (composed of target and projectile) such as has been suggested previously for lighter systems as a doorway to fusion [21] or to explain experimentally observed large binary yields [22]. One can assume that the system, while still in the dinuclear stage, emits one α particle in the forward and backward directions. On the average the barriers will be smaller since now they belong to Al (target) or Br (projectile). We have done such calculations with the assumption that the preequilibrium shape emission will occur only for angular momenta in the entrance channel (J) larger than the critical value for fusion, J_c. For values of J less than J_c, the usual complete fusion process occurs. For the present calculations, we have used $J_{\max}$ of $85\hbar$ and a J_c of $65\hbar$. This value of J_c is ten units less than the one used for the CF calculations because it is necessary to reduce the CF contribution in order to introduce the preequilibrium component. Nevertheless, most of the comparisons shown here are for the energy spectra which depend

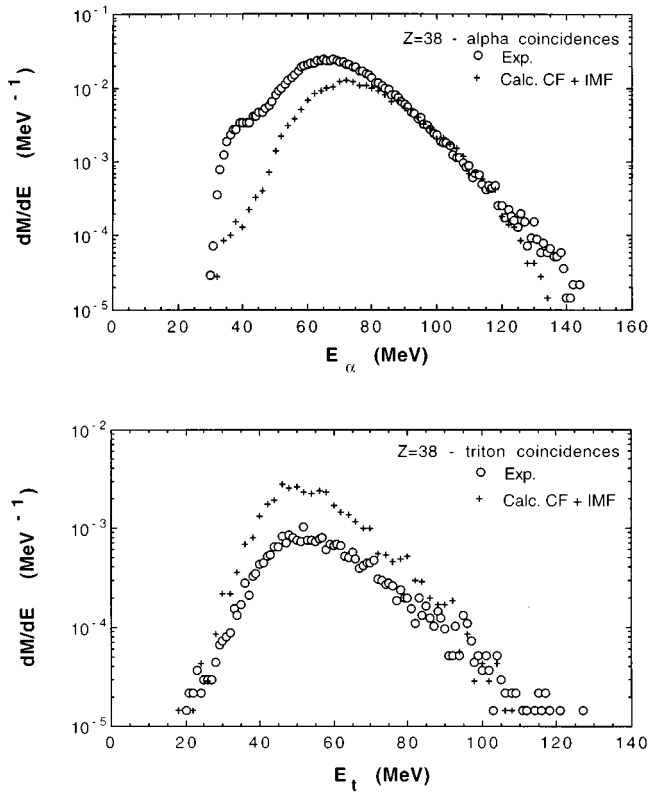

FIG. 21. Experimental energy spectra (circles) for tritons (bottom panel) and α's (top panel) in coincidence with $Z=38$. The calculations (crosses) are for a complete fusion process assuming all decay channels (mainly light particles and IMF's up to $Z=20$).

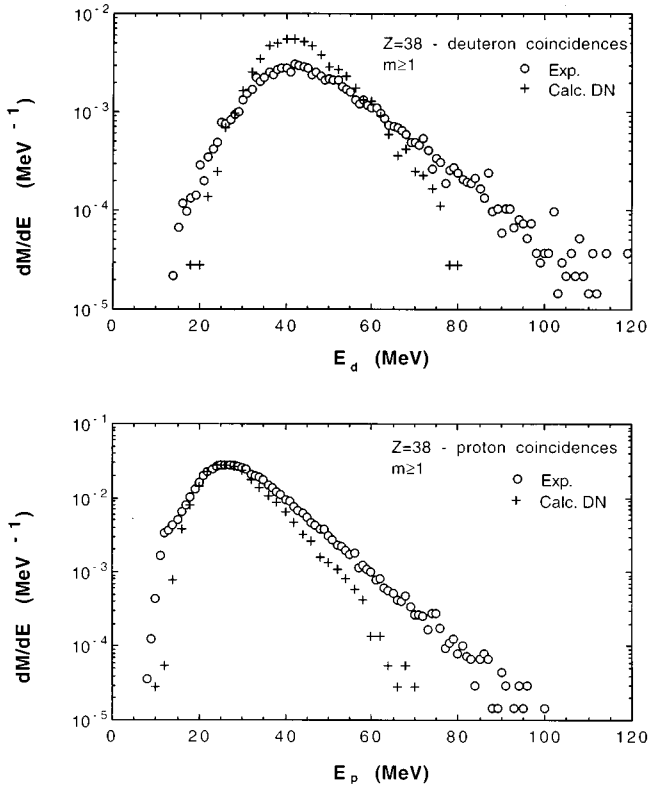

FIG. 22. Experimental energy spectra (circles) for protons (bottom panel) and deuterons (top panel) in coincidence with $Z=38$. The calculations (crosses) are for a process assuming emission from a dinuclear system prior to complete fusion and equilibration.

very little on small changes of J_c. The emission of n, p, d, t, and α was computed from the dinuclear configuration until the residual angular momenta value fell below J_c, at which point the system undergoes fusion and continues the usual equilibrium decay. The calculations were done using the level density $A/12$ and the code LILITA modified to accommodate the dinuclear step.

Results of the dinuclear calculation for the light-particle spectra in coincidence with $Z=38$ are shown in Fig. 22 for p and d and in Fig. 23 for t and α. The most important result of this calculations is for the α-particle emission (top panel of Fig. 23) where one can see that the fit has been greatly improved with respect to the calculations shown in Figs. 10, 14, 18, and 21. This "preequilibrium" calculation differs from the more common one used at energies above 20 MeV/nucleon [23,24] in that it requires low-energy emission from the dinuclear system following full momentum transfer. The main difference from equilibrium emission is in the low emission barrier due to the dinuclear shape assumed. Also the overall features of the calculations shown in Figs. 22 and 23 for p, d, and t are significantly better than from the other calculations. The results of this calculation for the ER spectra are essentially the same as those shown in Fig. 12.

The persistence of the dinuclear configuration as a major reaction mechanism in heavy ion collisions for energies up to ~20 MeV/nucleon has been documented recently in Ref. [25].

F. Choices of transmission coefficients

Recently [17,26], it has been pointed out that the usual approach of using, in the statistical model calculations, transmission coefficients (T_l's) derived from optical model calculations which fit the elastic scattering of the decaying pair may not be adequate. In particular, for neutrons, protons, and deuterons, the fit to the elastic scattering always requires the introduction of the surface absorption terms (usually in the form of a derivative to the Woods-Saxon formula). This makes the T_l's fall off with increasing energy to values below unity (normally to values around 0.9–0.7). A typical case is shown in Fig. 24 for the case of a $l=4$ proton on ^{105}Ag where the solid line represents the transmission coefficients obtained using the potential given in Refs. [10], [26]. Using the same geometry as the real well, we have substituted the surface absorption term by volume absorption. The resulting T_l's are given by the crossed line and reach an asymptotic value of unity at high energy. Using T_l's obtained from volume absorption potential for n, p, and d, we repeated the calculations of complete fusion such as those shown in Figs. 7 and 8. The results are shown for p and d in coincidence with $Z=40$ in Fig. 25 where the calculated spectra have been arbitrarily normalized to the data. As can be seen from Fig. 25, the improvement of the calculated spectra at high energy for the p case is significant compared to the curve in Fig. 7. The deuteron case improves slightly, but still the fit is as poor as in Fig. 8. In Refs. [17], [26] other effects of the optical model approach, such as shape resonance and

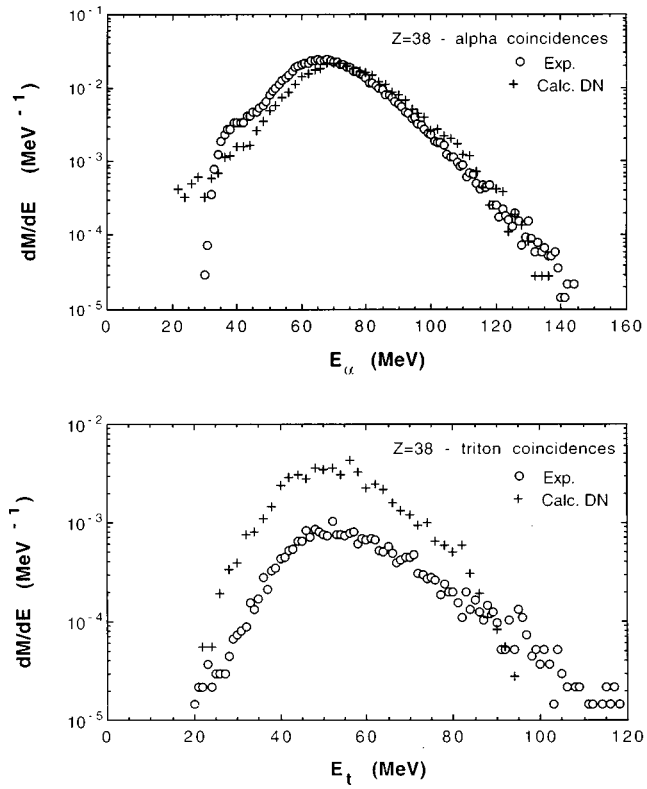

FIG. 23. Experimental energy spectra (circles) for tritons (bottom panel) and α's (top panel) in coincidence with $Z=38$. The calculations (crosses) are for α processes assuming emission from a dinuclear system prior to complete fusion and equilibration.

transparency, were investigated for all light particles (p, d, t, and α), and the authors proposed a simpler model IWBC (incoming wave boundary condition) for which the transmission is now only through a real potential and the imaginary part is substituted by ongoing wave boundary conditions inside the barrier. In the IWBC model the low-energy tails as well as the high-energy asymptotic behavior are modified. Evaluation of the effects of IWBC in the present calculation

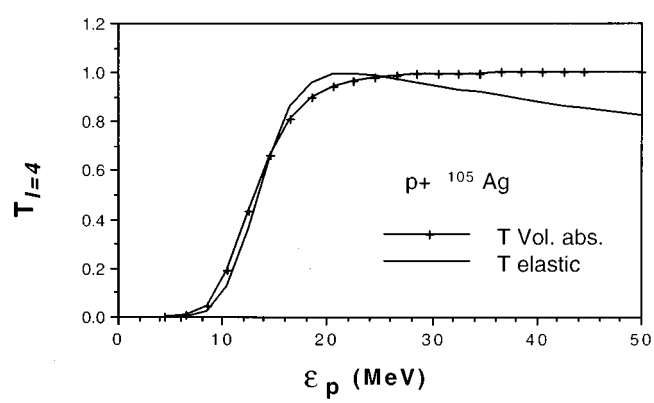

FIG. 24. Transmission coefficients (T_l) for $l=4$ for $p+^{105}$Ag. The solid line is obtained by using the optical model potential given in Ref. [10], and the crossed line is the same potential expected when the surface absorption term is substituted by volume absorption.

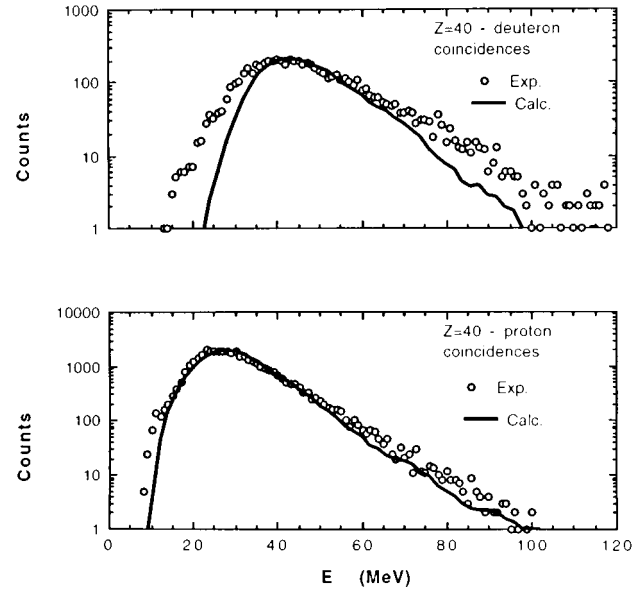

FIG. 25. Experimental energy spectra (circles) of p and d in coincidence with ER's of $Z=40$. The solid lines are the statistical model calculations for complete fusion but using the set of transmission coefficients with a volume absorption term for the optical potential of the kind shown in Fig. 24.

(other than the asymptotic behavior) is complicated because of other effects especially due to multiple emission (in fact, for $Z=38$ already ten charges are evaporated from the compound system) where uncertainties in level densities and other parameters strongly influence the calculated spectra. Regarding the high-energy behavior of the T_l's, one can say that for tritons and α's for which the optical model is already of the volume absorption type (i.e., $T_l \rightarrow 1$) the high-energy part is reasonably predicted (see Figs. 9, 10, 14, and 18), and therefore with all other parameters constant the predictions for p and d are indeed improved by imposing the asymptotic condition of $T_l=1$.

V. CONCLUSIONS

An analysis of the ER spectra obtained in coincidence with p, d, t, and α particles shows that complete fusion is the main component as expected from current systematics of complete-incomplete fusion deduced for lighter systems. In fact, it is shown that the ER spectra, analyzed in coincidence with light charged particles, have centroids which are consistent with complete fusion and a 10%–20% incomplete fusion component. However, the predicted widths of the ER spectra are narrower than the experimental values. By allowing also IMF evaporation to compete with light-particle emission, we can account for the width of the observed evaporation residue energy spectra.

The analysis of the light-particle spectra presents some difficulties in understanding the reaction mechanism. The centroids of the energy spectra of protons, deuterons, and tritons are generally consistent with expectations of complete-incomplete fusion mechanisms, but the α particles show much lower kinetic energies than expected. In addition, the experimental yields of deuterons and tritons are much smaller than the predicted values. The predicted high-energy

slopes of the energy spectra of p and d are too steep when a value of $A/8$ for the level density parameter is used; going to $A/12$ produces slopes that are in better agreement with the experiment. A preequilibrium shape emission mechanism which assumes full momentum transfer forming an intermediate dinuclear system, with emission from targetlike and projectilelike barriers for the light particles, can account for the lower energies of the α spectra, give a good fit for protons, and reasonable fits for deuterons and tritons. Slight improvements are observed for the high-energy tail of the proton and deuteron spectra using volume absorption for the optical model potential.

We have presented an analysis showing the effects of level densities, transmission coefficients, incomplete fusion, emission of IMF's, and preequilibrium shape emission, which are all relevant in determining the real mechanism involved in the emission of light particles and in the production of ER's. We have not achieved a unique description of the data or an overall description combining all these effects; however, we have shown that a successful description must consider several of them.

ACKNOWLEDGMENTS

Oak Ridge National Laboratory is managed by Lockheed Martin Energy Systems, Inc. under Contract No. DE-AC05-840R21400 with the U.S. Department of Energy. This work was also supported in part by NATO Grant No. CR6.890807d and by CONACYT (Mexico) Contract No. 1103-E9102.

[1] W. E. Parker, M. Kaplan, D. J. Moses, G. La Rana, D. Logan, R. Lacey, J. M. Alexander, D. M. de Castro Rizzo, P. DeYoung, R. J. Welberry, and J. T. Boger, Phys. Rev. C **44**, 774 (1991).

[2] M. Thoennessen, J. R. Beene, F. E. Bertrand, C. Baktash, M. L. Halbert, D. J. Horen, D. G. Sarantites, W. Spang, and D. W. Stracener, Phys. Rev. Lett. **70**, 4055 (1993).

[3] M. Beckerman, Rep. Prog. Nucl. Phys. **51**, 1047 (1988).

[4] D. Shapira, K. Teh, J. Blankenship, B. Burks, L. Foutch, H. J. Kim, M. Korolija, J. W. McConnell, M. Messick, R. Novotny, D. Rentsch, J. Shea, and J. P. Wieleczko, Nucl. Instrum. Methods Phys. Res. A **301**, 76 (1991).

[5] R. Wada, D. Fabris, K. Hagel, G. Nebbia, Y. Lou, M. Gonin, J. B. Natowitz, R. Billerey, B. Cheynis, A. Demeyer, D. Drain, D. Guinet, C. Pastor, L. Vagneron, K. Zaid, J. Alarja, A. Giorni, D. Heuer, C. Morand, B. Viano, C. Mazur, C. Ngô, S. Leray, R. Lucas, M. Ribrag, and E. Tomasi, Phys. Rev. C **39**, 497 (1989).

[6] A. Bracco, J. J. Gaardhøje, A. M. Bruce, J. D. Garrett, B. Herskind, M. Pignanelli, D. Barnéoud, H. Nifenecker, J. A. Pinston, C. Ristori, F. Schussler, J. Bacelar, and H. Hofmann, Phys. Rev. Lett. **62**, 2080 (1989).

[7] W. E. Ormand, P. F. Bortignon, A. Bracco, and R. A. Broglia, Phys. Rev. C **40**, 1510 (1989).

[8] J. Gomez del Campo and R. G. Stokstad, Report No. ORNL/TM-7295, 1981.

[9] J. P. Wieleczko, J. Gomez del Campo, D. Shapira, H. Kim, K. Teh, J. Shea, M. Korolija, C. Volant, and A. D'Onofrio, Physics Division Progress Report for Period Ending Sept. 30, 1989, No. ORNL-6578, p. 85.

[10] C. M. Perey and F. G. Perey, At. Data Nucl. Data Tables **17**, 1 (1976).

[11] J. R. Huizenga, A. N. Behkami, I. M. Govil, W. U. Schröder, and J. Töke, Phys. Rev. C **40**, 668 (1989).

[12] J. Gomez del Campo, J. L. Charvet, A. D'Onofrio, R. L. Auble, J. R. Beene, M. L. Halbert, and H. J. Kim, Phys. Rev. Lett. **61**, 290 (1988).

[13] W. F. W. Schneider, F. Pühlhofer, R. P. Chestnut, C. Volant, H. Freiesleben, W. Pfeffer, and B. Kohlmeyer, Nucl. Phys. **A371**, 493 (1981).

[14] H. Morgenstern, W. Bohne, W. Galster, K. Grabisch, and A. Kyanowski, Phys. Rev. Lett. **52**, 1104 (1984), and references therein.

[15] G. P. Gilfoyle, M. S. Gordon, R. L. McGrath, G. Auger, J. M. Alexander, D. G. Kovar, M. F. Vineyard, C. Beck, D. J. Henderson, P. A. DeYoung, and D. Kortering, Phys. Rev. C **46**, 265 (1992).

[16] M. F. Vineyard, J. S. Bauer, J. F. Crum, C. H. Gosdin, R. S. Trotter, D. G. Kovar, C. Beck, D. J. Henderson, R. V. F. Janssens, B. D. Wilkins, C. F. Maguire, J. F. Mateja, F. W. Prosser, and G. S. F. Stephens, Phys. Rev. C **45**, 1784 (1992).

[17] N. G. Nicolis, D. G. Sarantites, L. G. Sobotka, and R. J. Charity, Phys. Rev. C **45**, 2393 (1992).

[18] M. Gonin, L. Cooke, K. Hagel, Y. Lou, J. B. Natowitz, R. P. Schmitt, S. Shlomo, B. Srivastava, W. Turmel, H. Utsunomiya, R. Wada, G. Nardelli, G. Nebbia, G. Viesti, R. Zanon, B. Fornal, G. Prete, K. Niita, S. Hannuschke, P. Gonthier, and B. Wilkins, Phys. Rev. C **42**, 2125 (1990).

[19] K. Yuasa-Nakagawa, Y. H. Pu, S. C. Jeong, T. Mizota, Y. Futami, S. M. Lee, T. Nakagawa, B. Heusch, K. Ieki, and T. Matsuse, Phys. Lett. B **283**, 185 (1992).

[20] J. Gomez del Campo, R. L. Auble, J. R. Beene, M. L. Halbert, H. J. Kim, A. D'Onofrio, and J. L. Charvet, Phys. Rev. C **43**, 2689 (1991).

[21] M. S. Hussein, B. V. Carlson, O. Civitarese, and A. Szanto de Toledo, Phys. Rev. Lett. **54**, 2659 (1985).

[22] D. Shapira, D. Schull, J. L. C. Ford, Jr., B. Shivakumar, R. L. Parks, R. A. Cecil, and S. T. Thornton, Phys. Rev. Lett. **53**, 1634 (1984).

[23] A. D'Onofrio, J. Gomez del Campo, B. Delaunay, J. Delaunay, H. Dumont, F. Andreozzi, A. Brondi, R. Moro, M. Romano, and F. Terrasi, Phys. Rev. C **39**, 834 (1989).

[24] M. Blann, Phys. Rev. C **31**, 1245 (1985).

[25] S. P. Baldwin, B. Lott, B. M. Szabo, B. M. Quednau, W. U. Schröeder, J. Tôke, L. G. Sobotka, J. Barreto, R. J. Charity, L. Gallamore, D. G. Sarantites, D. W. Stracener, and R. T. de Souza, Phys. Rev. Lett. **74**, 1299 (1995).

[26] J. M. Alexander, M. T. Magda, and S. Landowne, Phys. Rev. C **42**, 1092 (1990).